

opportunity to develop agricultural systems based on regular water supplies. Irrigation often represents a large part of crop water-use in these areas due to the dry conditions that prevail during the growing season (Siebert and Döll, 2010).

This makes such systems highly vulnerable to projected changes in climate conditions, for at least two reasons. First, warmer temperatures will reduce the fraction of precipitation falling as snow and tend to accelerate snowmelt, leading to earlier and reduced spring peak flows and increased winter flows (Adam et al., 2009; Sproles et al., 2013). Reduced summer and fall flows could in turn significantly impact water availability for irrigation purposes. Second, higher temperatures in the valleys will affect the timing of phenological events (Cleland et al., 2007), which drive the seasonal pattern of crop water needs. Some perennial crops like grapevines are already showing a tendency toward earlier events and shortened growth intervals in many regions of the world (Jones et al., 2005; Duchêne et al., 2010a). Vineyards located in semi-arid mountainous areas are particularly exposed, owing to high diurnal temperature variations and overall sub-optimal growing temperatures (Caffarra and Eccel, 2011). It has also been noted that elevated temperatures may adversely affect the ability to meet chilling requirements during the crop dormancy (Webb et al., 2007).

Thus, the future of agricultural systems in snow-dominated, semi-arid catchments relies on our ability to anticipate the complex relationships between climate conditions, snowmelt timing, water availability and crop water-use.

1.1 Advantages and limitations of current conceptual precipitation-runoff models

To understand and forecast the response of hydrological systems, hydrologists often rely on numerical catchment models known as “conceptual precipitation-runoff models”. Precipitation inputs are processed into runoff through a number of inter-connected water stores representing different aspects of the system’s behavior (e.g. slow vs. fast responses, surface-water vs. groundwater compartments). In general, relatively simple structures are used, in which typically less than 10 parameters require calibration

11487

against physically observable responses (e.g. streamflow data) (Wagener et al., 2001). Such models also have low data and computer requirements, making them especially attractive in data-scarce areas such as remote mountainous catchments. As a result, they are being increasingly used to evaluate the potential impacts of land-use and/or climate changes on the capacity to meet agricultural water demands (e.g. Merritt et al., 2004; Collet et al., 2015; Fabre et al., 2015a).

The conclusions drawn from these models, however, are naturally bounded by a range of uncertainty arising from multiple sources of error and approximations. This includes the impacts of input data errors, numerical approximations, structural inadequacies and model non-uniqueness. Parameter instability under changing climate and/or anthropogenic conditions represents an additional source of uncertainty that may be difficult to distinguish from parameter equifinality in the absence of uncertainty analysis (Siebert and McDonnell, 2010; Brigode et al., 2013). Such limitations remain largely overlooked in many impact studies. Instead, it is often assumed that the uncertainty associated with climate and/or water-use scenarios greatly outweighs that arising from the modeling process itself. From a water management perspective, however, the added value of precipitation-runoff models lies not simply in their ability to provide accurate streamflow predictions but also in the systematic examination of the uncertainty surrounding these predictions and the ultimate decision being addressed (Ajami et al., 2008).

One of the most effective means of providing such information is through the use of Bayesian inference methods. Notwithstanding some real issues in how best to handle epistemic uncertainties, and whether probability theory is the right tool to use (Beven et al., 2011; Montanari, 2011), formal Bayesian approaches offer the opportunity to test the reliability of model predictions through a series of posterior diagnostics. This, in turn, provides a meaningful way to discuss the relative merits of competing model structures or different versions of the same model. Very often, structural inadequacies can be partially alleviated by comparing alternative representations of the processes at work. This paper addresses two specific issues pertaining to the use of conceptual

11488

of snowmelt estimates under higher temperatures (e.g. Boudhar et al., 2009; Ayala et al., 2015).

1.4 Objectives

Ideally, the incorporation of new processes into a given model structure should be achieved using the same level of mathematical abstraction and process representation as in the original model. Blöschl and Montanari (2010) insisted that “a better understanding of the hydrological processes should not necessarily translate into more complex models used in impact studies”. Indeed, maintaining low-dimensional, holistic modeling approaches is essential to constrain parameter uncertainty and help the modelers focus on understanding the main drivers of hydrological change.

This paper investigates one possible way of integrating the effects of irrigation water-use and snow sublimation into a parsimonious, catchment-scale modeling framework. These processes are typically not accounted for in currently available precipitation-runoff models. Particular attention is paid to the representation of changes in irrigated areas and crop varieties over time. The method is tested in a snowmelt-fed catchment of the Coquimbo region, in Chile. This semi-arid region is currently facing one of the worst droughts in its recorded history, causing a significant decrease in water availability for agriculture (Salinas et al., 2015).

2 Study area and data

2.1 General setting

2.1.1 Physical landscape

The Claro River catchment is a semi-arid, mountainous catchment located in North-Central Chile (30° S). It drains an area of about 1515 km² characterized by a series of granitic mountain blocks interspersed with steep-sided valleys. Elevations range from 11491

820 m a.s.l. at the catchment outlet in Rivadavia to approximately 5500 m a.s.l. near the border with Argentina (Fig. 1a). Above 3000 m a.s.l., repeated glaciations and the continuous action of frost and thaw throughout the year have caused an intense shattering of the exposed rocks, leaving a landscape of bare rock and screes almost devoid of soil. The valley-fill material consists of mostly unconsolidated glaciofluvial and alluvial sediments mantled by generally thin soils (< 1 m) of sandy to sandy-loam texture. Natural vegetation outside the valleys is extremely sparse and composed mainly of subshrubs (e.g. *Adesmia echinus*) and cushion plants (e.g. *Laretia acaulis*) with very low transpiration rates (Squeo et al., 1993; Kalthoff et al., 2006). In the lower part of the catchment, vineyards and orchards cover most of the valley floors and lower hill slopes, where they benefit from a unique combination of clear skies, high diurnal temperature variations and overall dry conditions during the growing season. The Claro River originates from a number of small, snowmelt-fed tributaries flowing either permanently or seasonally in the mountains.

2.1.2 Climate

Most of the annual precipitation falls as snow during typically 2 or 3 winter storms (Favier et al., 2009), when the South Pacific High reaches its northernmost position (June–August). Mean annual precipitation ranges from approximately 100 mm at the catchment outlet (Rivadavia) to 670 mm in the High Cordillera (Bourgin et al., 2012). The annual snow cover duration estimated from MODIS snow-covered area (SCA) data (see Sect. 2.2) ranges from less than 20–40 days at low elevations (< 2000 m a.s.l.) to about 160–180 days at high elevations (> 4000 m a.s.l.), where sublimation is expected to be the dominant cause of ablation (Gascoïn et al., 2013; MacDonell et al., 2013). In the dry Andes, net shortwave radiation represents the dominant source of energy available for melt and sublimation (Pelliciotti et al., 2008).

At the inter-annual timescale, the El Niño Southern Oscillation (ENSO) represents the largest source of climate variability (Montecinos and Aceituno, 2003). Anomalously wet (dry) years in the region are generally associated with warm (cold) El Niño (La

Niña) episodes and a simultaneous weakening (strengthening) of the South Pacific High. It is worth noting, however, that some very wet years in the catchment can also coincide with neutral to weak La Niña conditions, as in 2000–2001, while several years of below-normal precipitation may not exhibit clear La Niña characteristics (Verbist et al., 2010). These anomalies may be due to other modes of climate variability affecting the Pacific basin on longer timescales. The Interdecadal Pacific Oscillation (IPO), in particular, has been shown to modulate ENSO's influence according to cycles of 15 to 30 years (Schulz et al., 2011). Figure 1c shows a sustained decrease in mean annual streamflow since the mid-1990s, which could be associated with a shift in the IPO phase around 1998.

2.1.3 Agricultural activity

Grape growing is by far the main agricultural activity in the catchment. All grapes are grown to be exported as early-season table grapes or processed into a brandy-like national drink known as *pisco*. Reliable water supplies are critical to satisfy crop water needs in the summer, since precipitation events occur mostly at high elevations or outside the growing season. Irrigation water is diverted at multiple locations along the river's course and conveyed to the fields through a complex network of open, mostly unlined canals. The amount of water diverted from the river depends on both historical water rights and current water availability. Table varieties are mostly drip-irrigated while pisco varieties remain largely furrow-irrigated.

Irrigated areas in the Claro River catchment have increased by about 200 % between 1985 and 2005 (Fig. 1b). This expansion has been limited by both water and agricultural land availability, and irrigated areas currently represent less than 5 % of the total catchment area. A rough estimate of the effects of increased irrigated areas on mean annual streamflow can be obtained by looking at the difference in discharge measured at Rivadavia (downstream from cultivated areas) and that measured at Cochiguaz and Alcohuz (upstream from cultivated areas) (Fig. 1c). Note that transmission losses

11493

caused by evaporation and infiltration through the riverbed also reduce streamflow at downstream points, especially during dry periods when the depth of water tables is low.

2.2 Materials

2.2.1 Hydro-climate data

Precipitation and temperature data were interpolated from respectively 12 and 8 stations to a 5 km × 5 km grid using an inverse distance squared weighting (Ruelland et al., 2014). Orographic effects on precipitation were considered using the approach described in Valéry et al. (2010a) with a correction factor of $6.5 \times 10^{-4} \text{ m}^{-1}$ (determined by sensitivity analysis), resulting in a gradient of around 0.4 m we km^{-1} . For temperature, a constant lapse rate of $-6.0 \text{ }^\circ\text{C km}^{-1}$ was estimated from the observed data. Daily streamflow data were extracted from the Chilean *Dirección General de Aguas*' database.

In addition, remotely-sensed data from the MODerate resolution Imaging Spectroradiometer (MODIS) sensor were introduced to estimate the seasonal patterns of fractional snow-covered areas (F_{SCA}) over a 12 year period (2000–2011). Daily snow cover products retrieved from NASA's Terra (MOD10A1) and Aqua (MYD10A1) satellites were combined into a single, composite 500 m resolution product to reduce the effect of swath gaps and cloud obscuration. The remaining data voids due to cloud cover or missing data were subsequently filled using a linear temporal interpolation method, where a pixel was classified as snow/land depending on the closest previous/next observation of snow/land.

2.2.2 Agricultural data

Two different grapevine varieties were selected to represent phenological patterns in the valleys, namely: Flame Seedless (for table grapes) and Moscatel Rosada (for pisco grapes). Phenological observations for these two varieties were carried out over a 10–

11494

year period (2003–2012) at the *Instituto de Investigaciones Agropecuarias* (INIA), located a few kilometers downstream from the catchment outlet. Grapevines were trained using an overhead trellis system and fully irrigated during the whole growing season. The experiment kept track of three major events: budburst (BB), full bloom (FB) and the beginning of harvest (HV). Budburst was defined as the moment when the first leaf tips become visible and full bloom as the moment when 80 % of the flower caps are off. The beginning of harvest depends on the intended use of the grapes. Table varieties require lower sugar contents ($\sim 16^\circ$ Brix) than those dedicated to the production of pisco (22° Brix), which are generally harvested a few months later (Ibacache, 2008).

A database of water access entitlements was used to estimate the total volume of water licensed for abstraction in the catchment. This included a time series of monthly restrictions to these entitlements issued by the *Dirección General de Aguas* during prolonged dry periods.

3 Methods

3.1 Modeling framework

In this paper we developed and compared three different models. These differed in their approach to snowmelt and irrigation modeling. The first one, referred to as “Model A”, used a simple degree-day approach to estimate snowmelt rates while neglecting the effects of irrigation water-use (IWU) at the catchment scale. The second one, referred to as “Model B”, ignored IWU effects just as Model A but relied on an enhanced degree-day approach to account for the effects of net radiation and sublimation on melt rates. The third one, referred to as “Model C”, used the same snowmelt routine as Model B and incorporated IWU effects on natural streamflow using a conceptual irrigation module.

Figure 2 shows a block diagram of this modeling framework. The blue blocks refer to the hydrological part of the framework shared by the three models (see Sects. 3.1.2.

11495

and 3.1.3). The green blocks relate to the estimation of irrigation water requirements (IWR) used only by Model C. This involves several phenological models to capture the main dynamics of crop water needs over each growing season (Sect. 3.1.4) and a moisture-accounting store representing the valley soils (Sect. 3.1.3). Net irrigation water-use at the catchment scale is computed as a function of IWR, irrigated areas and water availability (i.e. natural streamflow) (Sect. 3.1.3). The whole modeling chain is fed by precipitation and temperature data.

We also stress that smoothing functions were used throughout this framework to remove all threshold nonlinearities from the models’ equations (insofar as possible), as recommended by several authors (e.g. Fenicia et al., 2011). These smoothing functions will not be shown in the following sections for the sake of clarity.

3.1.1 Simplifying assumptions

The modeling framework described in Fig. 2 relies on three important assumptions regarding the representation of IWU and IWR at the catchment scale:

1. First, IWU refers to the amount of water lost by evapotranspiration from the cropped fields and the riparian vegetation that thrives along the irrigation canals. It should not be confused with the actual surface-water withdrawals (SWW) that vary on a weekly or monthly basis depending on historical water rights and planning/management decisions. SWW include IWU but also non-consumptive losses caused by canal seepage and deep percolation in the fields. Unfortunately, the impact of SWW on the catchment behavior is difficult to estimate because reliable information on these additional losses and the proportion of abstracted flows coming back to the system is lacking. In this study, all return flows were assumed to come back to the river within each time step. A similar assumption can be found in Kiptala et al. (2014).

2. Second, IWR refer to the amount of water needed to satisfy crop evapotranspiration under optimal conditions. In practice, this quantity depends on the irrigation

11496

where N_C is the number of grid cells, N_Z is the number of elevations zones (Z), λ_v is the latent heat of vaporization ($\sim 2.46 \text{ MJ kg}^{-1}$) and $PE_{\text{Oudin},C}$ (mm) is given by Eq. (11). Note that PE_{GR4J} accounts for evapotranspiration from soils, natural vegetation and crops only insofar as it relates to precipitation or meltwater. It is not supposed to include evapotranspiration from cultivated areas caused by irrigation water-use. Thus, the GR4J model simulates only those hydrological processes that relate to the “natural” catchment behavior. Incorporation of IWU in the modeling framework does not modify the structure and governing equations of the GR4J model but only the estimates of natural streamflow. This choice can be justified by the fact that the cultivated areas concentrate mainly in the lower part of the catchment and represent only a small portion of the total area (Fig. 1).

The GR4J model was chosen for its simplicity and parsimony. Basically, the precipitation-runoff process is broken down into two components: a runoff generation module computes the amount of water available for runoff, i.e. “effective precipitation”, while a routing module subsequently routes this quantity to the catchment outlet. In the first module, a soil-moisture accounting (SMA) store is used to partition the incoming rainfall and/or snowmelt into storage, evapotranspiration and excess precipitation. At each time step, a fraction of the SMA store is also computed to represent soil drainage and added to excess precipitation to form the effective precipitation. The second module splits this quantity between two different pathways with respect to a constant ratio: 10 % passes as direct runoff through a quick flow routing path based on a unique unit hydrograph whereas 90 % passes as delayed runoff through a slow flow routing path composed of a unit hydrograph and an additional routing store. Outputs from both pathways are finally added up to simulate natural streamflow at the catchment outlet. This model relies on four calibrated parameters (X_1 , X_2 , X_3 and X_4) that are described in Table 1.

11501

3.1.4 Irrigation water-use module (Model C)

In Model C, irrigation water requirements per unit area (IWR, in mm day^{-1}) were estimated for each crop variety i using a simple soil-water balance approach:

$$\text{IWR}_i = \max[0, \text{ETM}_i - \text{SWC}_i - R_{\text{Valley}}] \quad (13)$$

$$\text{with } \text{ETM}_i(T_{A,V}) = K_{C,i} \text{ET}_0(T_{A,V}) \quad (14)$$

where ETM (mm day^{-1}) refers to crop evapotranspiration under optimal conditions and SWC (mm) to the average soil-water content in the root zone. R_{Valley} (mm day^{-1}), ET_0 (mm day^{-1}) and $T_{A,V}$ ($^{\circ}\text{C}$) are respectively the areal effective precipitation, reference evapotranspiration and air temperature in the valleys, and K_C is a coefficient depending on crop growth stages. A realistic estimate of ET_0 was provided by using a modified version of Oudin’s formula (Eq. 11). In Oudin et al. (2005), the values of K_1 and K_2 were chosen as those giving the best streamflow simulations for different hydrological models applied to a large number of catchments. In this study, the FAO Penman–Monteith equation for a reference grass was used as a basis to re-calibrate these parameters at different locations across the valleys. This modification was required since the Penman–Monteith equation, which was more suited to estimating crop water needs, could not be used over the whole study period due to limited data availability (wind speed, relative humidity, solar radiation). Interpolated K_C curves were constructed for each crop variety using a series of phenological models to simulate the annual dates of budburst, full bloom, harvest and leaf fall (see Sect. 3.1.5). The value of K_C at each of these dates ($K_{C,\text{BB}}$, $K_{C,\text{FB}}$, $K_{C,\text{HV}}$ and $K_{C,\text{LF}}$) was determined from the literature (Villagra et al., 2014) and interviews with local grape growers. Net irrigation water-use in the catchment (IWU, in $\text{m}^3 \text{ s}^{-1}$) was computed as a function of IWR, irrigated areas and surface-water availability:

11502

The 4-parameter model developed by Wang and Engel (1998) (hereafter referred to as WE) was selected to simulate the annual dates of full bloom (t_{FB}) and harvest (t_{HV}):

$$F_{FB} = \sum_{t=t_{BB}}^{t_{FB}} R_{FB}(T_{A,V}) \text{ and } F_{HV} = \sum_{t=t_{FB}}^{t_{HV}} R_{HV}(T_{A,V}) \quad (22)$$

$$R_{FB}(T_{A,V}) = R_{HV}(T) = \begin{cases} \frac{2(T_{A,V}-T_{min})^\alpha (T_{opt}-T_{min})^\alpha - (T_{A,V}-T_{min})^{2\alpha}}{(T_{opt}-T_{min})^{2\alpha}} & \text{if } T_{min} \leq T_{A,V} \leq T_{max} \\ 0 & \text{otherwise} \end{cases} \quad (23)$$

$$\text{with } \alpha = \log(2)/\log[(T_{max} - T_{min})/(T_{opt} - T_{min})] \quad (24)$$

where F_{FB} , F_{HV} and T_{opt} ($^{\circ}\text{C}$) were calibrated separately for each variety. Note that T_{opt} also varies with the phenophase under study (flowering or ripening). Compared to other flowering and harvest models based on forcing rates, this one has the major advantage of also accounting for the inhibiting effect of extreme temperatures on photosynthesis. As leaf growth typically ceases at temperatures below 0–5 $^{\circ}\text{C}$ (Hendrickson et al., 2004) and above 35–40 $^{\circ}\text{C}$ (Greer and Weedon, 2013), parameters T_{min} and T_{max} were fixed beforehand at 0 and 40 $^{\circ}\text{C}$ respectively (García de Cortázar-Atauri et al., 2010).

Eventually, the post-harvest period was modeled as a constant number of days (N_{LF}) between t_{HV} and the end of leaf fall (t_{LF}). The value of N_{LF} was obtained from interviews with local grape growers for each variety (see Table 1).

3.2 Model evaluation

The phenological and hydrological models were evaluated separately using different methods and/or objective functions. Models A and B have the same number of calibrated hydrological parameters (i.e. 6 parameters).

11505

3.2.1 Hydrological modeling

The dataset was divided into a calibration period (1985–1995), showing a sharp increase in irrigated areas (+100%), and a validation period (1995–2005), characterized by a much lower increase (+20%) (Fig. 1b). Each period was defined in terms of water years (from 1 May to 30 April) and included at least one major El Niño (1987–1988, 1997–1998 and 2002–2003) or La Niña (1988–1989, 1998–1999 and 1999–2000) event.

The models were evaluated using either (1) simulations obtained with a single, “optimal” parameter set, or (2) probabilistic predictions obtained by sampling the posterior distributions of the parameters. In the first case, model efficiency and internal consistency were assessed. In the second case, predictive uncertainty bands were derived and scrutinized in terms of reliability and sharpness.

Model efficiency and internal consistency

Model efficiency measures the ability to fit the observed behavior of the system with regard to specific criteria. In this study, the Shuffle Complex Evolution (SCE) algorithm (Duan et al., 1993) was used to maximize the following criterion:

$$F_{obj} = (KGE + KGE_{inv})/2 \quad (25)$$

where KGE and KGE_{inv} refer to the Kling-Gupta Efficiency (Gupta et al., 2009) computed from discharge (Q) and inverse discharge ($1/Q$) values respectively. This composite criterion was chosen to emphasize high and low flows equally (Pushpalatha et al., 2012; Nicolle et al., 2014).

Internal consistency can be defined as the ability to reproduce the dynamics of internal catchment states without conditioning the model parameters on additional data. Here, this analysis was limited to the Snow Accumulation and Ablation module to evaluate its ability to reproduce the seasonal pattern of snow storage and release within each elevation zone. This was achieved through visual inspection of model-based and

11506

4 Results

4.1 Phenological simulations

Figure 5, Tables 2 and 3 show the results obtained for both grapevine varieties with the three phenological models. On the whole, approximately 76% of the differences between observed and predicted phenological dates fell within the range of ± 5 days during calibration (Fig. 5). Moreover, mean absolute errors did not exceed 6.4 days in any case. Such errors can be considered acceptable with regard to the 10 day time step chosen to evaluate the hydrological models.

The best results were obtained for Flame Seedless with the budburst (BB) model and for Moscatel Rosada with the full bloom (FB) and harvest (HV) models. RMSE values ranged from 3.0 to 6.1 days in calibration and from 5.4 to 7.9 days in validation, indicating a moderate loss of performance (Table 2). In general, bias values remained close to zero, except for Moscatel Rosada with the HV model. NSE values were positive for all varieties and models in calibration but decreased sharply in validation, with only two values above 0.50 and one negative value for Flame Seedless with the FB model. However, very low to negative NSE values are not uncommon in phenological modeling when only a few observations (< 10 years) collected from a single site are used to calibrate the models (e.g. Parker et al., 2013). The optimized parameter values displayed in Table 3 are discussed in Sect. 5.4.

4.2 Hydrological simulations

4.2.1 Model efficiency and internal consistency

Table 4 show the results obtained from the calibration and validation of Models A, B and C. Clearly, Model C was found to perform better than Models A and B with respect to the objective function given by Eq. (25). This higher performance was mostly the result of improved low-flow simulations (KGE_{inv}). Table 5 shows that simulated sublimation

11509

rates and contribution to snow ablation remained approximately the same when IWU was introduced in the model equations. Estimated mean annual sublimation rates at high elevations (EZ no. 4 and 5) were consistent with those found by other studies, including experimental studies conducted on small glaciers of the region (MacDonell et al., 2013).

The internal consistency of the SAA module was verified over an independent validation period (2000–2011) using the parameters (θ_S , MF) calibrated with each Model from 1985 to 1995. The snow errors displayed in Table 4 vary from 2% in the first elevation zone (EZ no. 1) to 11–17% in the last one (EZ no. 5). Such errors were very encouraging, as they were comparable to those obtained by Hublart et al. (2015) in the same catchment with less parsimonious (and less realistic) snowmelt models. The impact of considering net radiation and sublimation in the model equations, however, was only evident for EZ no. 4 and 5, where a moderate drop in the snow error was observed. Model A even performed slightly better than Model B with respect to the F_{obj} function, showing that (supposedly) improved internal consistency (and model realism) may not necessarily go with improved model performance when looking at the system's integrated response (i.e. streamflow).

Figure 6 provides a visual comparison of simulated and observed fractional snow-covered areas (F_{SCA}) during this validation period for Model C. On the whole, it can be seen that the SAA model did not accumulate snow from one year to another, which was consistent with the observed inter-annual pattern of snow cover in the catchment. However, there were important discrepancies between the lower and upper elevation zones. In the lower zones (EZ no. 2 and 3), the model did fairly well during several years of the period (e.g. 2001, 2004, 2009 and 2010) but also under-estimated the annual snow cover duration (SCD) during several other years (e.g. 2002, 2003 and 2007). In the upper zones (EZ no. 4 and 5), the model generally failed to reproduce the observed variations in F_{SCA} despite improved estimates of the annual SCD. In EZ no. 5, there was also a tendency to over-estimate the SCD during the last 3–4 years of the period.

11510

4.2.2 Model predictive uncertainty

Between 10 000 and 13 000 model evaluations were required to reach convergence to a limiting distribution depending on the Model used. In each case, the last 5000 samples generated with DREAM were used to compute the posterior diagnostics presented in Sect. 3.2.1. and generate predictive uncertainty bands.

Figure 7 provides a range of formal tests of the statistical assumptions made to describe model residuals in the case of Model C. The density plot of Fig. 7a confirms that model residuals were broadly symmetric and kurtotic, although kurtosis appears to be slightly overestimated. Heteroscedasticity (Fig. 7c) was largely removed by the variance model of the GL function. However, Fig. 7b shows that the assumption of independence was not fully respected, as residuals remained slightly correlated (0.35) at a lag of 1 and at some greater lags, indicating potential storage errors in the model structure.

Figure 8 displays the scatter plots and posterior histograms of hydrological parameters for Models A and C. The results obtained with Model B are not shown here as they were generally close to those of Model C. As can be seen, differences between the structures of Models A and C had no particular effect on parameter identifiability. All parameters appeared to be relatively well-defined with approximately Gaussian distributions, although the values of θ_S , MF and X3 occupied a wider range of their prior intervals with Model A than with Models B and C. Introducing sublimation and net radiation in the SAA module reduced the correlation between θ_S and MF observed with Model A but simultaneously increased the interaction of θ_S with X3 and X4. Likewise, additional checks performed with Models B and C showed that the strong correlation between X2 and X3 observed for Model C was mainly due to the incorporation of irrigation water-use in the modeling framework.

Figure 9 shows the posterior diagnostics used to evaluate the reliability (PIT, POCI) and resolution (ARIL) of forecast distributions for Models B and C. At first sight, the PIT values obtained with all streamflow observations appear to be distributed quite uni-

11511

formly during both simulation periods. Small departures from the diagonal line and the 5 % Kolmogorov confidence bands indicate a tendency to under-predict the observed data, but this applies to both models, especially in validation. On the contrary, significant differences between the two models become obvious when looking at specific portions of the observed flow duration curve. At low flows, the PIT values obtained with Model B revealed a significant over-prediction bias during both calibration and validation periods. While it did not affect the percentage of observations covered by the confidence intervals (as POCI values remained close to the diagonal line), this systematic bias resulted in very high ARIL values (exceeding 1.5 in calibration and 3 in validation with the 95 % confidence intervals). By contrast, Model C slightly over-estimated predictive uncertainty in calibration but led to highly reliable low-flow predictions in validation, as evidenced by the PIT and POCI plots. This resulted in relatively low ARIL values (< 1). At mid-flows, the two models exhibited a similar behavior characterized by a systematic under-prediction bias, under-estimated POCI values and relatively low ARIL values (< 1). At high flows, the PIT values were well within the Kolmogorov confidence bands for both models, although there was still a tendency to under-predict the observed data. In validation, this under-prediction bias translated into an excessively low number of observations enclosed within any p -confidence interval for $p > 70\%$.

Figure 10 shows the uncertainty bands obtained with Models B and C during the two simulation periods. The dark blue region represents the uncertainty in streamflow predictions associated with the posterior parameter distributions while the light blue region represents the total uncertainty arising from parameter, model structure and input errors simultaneously. Some portions of the observed hydrograph have been enlarged to highlight key differences between the two models. In general, uncertainty bands should be wide enough to include the expected percentage of streamflow observations (here, 95 %), but no so wide that the representation of the observed hydrograph becomes meaningless. From this perspective, the main differences between Models B and C were observed for summer flows, i.e. during the irrigation season. Model B results in large uncertainty bands that are able to capture most of the observations

11512

0 °C for a sufficiently long period of time. Another possible explanation is that a high value of θ_S implicitly accounts for the effect of night-time freezing, which further delays snowmelt despite warm day-time temperatures. At high elevations (> 4000 m a.s.l., i.e. EZ no. 5), where observed air temperatures are mostly negative, we note that a constant lapse rate of 6.0 °C km^{-1} , as applied in this study for all elevation zones, was also likely to over-estimate temperature inputs. Lapse rates at these elevations are generally much greater than that, being in fact closer to the dry adiabatic lapse rate. Again, this would be expected to generate high values of θ_S to compensate for temperature over-estimation.

The main drawback of this approach (i.e. using air temperature as a proxy for the snowpack cold-content) is that it remains largely implicit and only indirectly connected to the amount of water lost by sublimation in the model (i.e. the outcome of Eq. 10 has no effect on Eq. 2). This does not mean, however, that a physically-oriented interpretation cannot be sought a posteriori to check for the model realism. Alternative approaches can also be used to account for the delay in meltwater production at the start of the ablation season. In general, these will involve an additional store representing the water-holding capacity of the snowpack (Schaeffli and Huss, 2011). Although further research would be required to compare the relative merits of each approach, the representation chosen in this study may be more suited to catchments with shallow snowpacks and significant sublimation.

The “optimal” melt factor (MF) was significantly higher with Model A than with Models B and C (Fig. 7). This was not surprising since, in the case of Models B and C, the effects of net radiation were explicitly considered and the melt factor was meant to parameterize only the contribution of turbulent energy fluxes. Such a “restricted” melt factor is expected to increase with increasing wind speed and/or relative humidity, as shown by Brubaker et al. (1996). The relatively low values ($\sim 2\text{ mm day}^{-1}$) obtained here were therefore consistent with the overall dry conditions of the study area. However, we found little evidence of improved model performance and internal consistency when a restricted melt factor was used and net radiation and sublimation were intro-

11515

duced in the model equations (see Table 4). This lack of sensitivity may be due to other sources of uncertainty, in particular regarding the choice of an adequate snow depletion curve to estimate fractional snow-covered areas (Eq. 6).

While most snowmelt routines used in conceptual catchment models assume either entirely snow-free or entirely snow-covered elevation zones, accounting for the proportion of each zone over which snow extends can be critical where mean snow depths are known to be small. As a first approximation, we relied on a linear relationship between SWE and F_{SCA} that did not account for wind redistribution effects or differences in radiation receipt caused by slopes of different aspects. In the dry Andes, wind-induced redistribution has been shown to significantly increase the spatial variability in snow depth, hence reducing the total snow cover area during winter (Gascoin et al., 2013; Ayala et al., 2014). For a proper assessment of predictive uncertainty, a multi-criteria likelihood function accounting for the differences between several types of simulated and observed responses (typically, fractional snow-covered areas and stream flows) should be used (e.g. Koskela et al., 2012). This is the subject of ongoing research.

5.3 Runoff generation and routing

Figures 9 and 10 revealed a clear under-prediction bias in the simulation of winter and early spring flows during several water years. Further details on these systematic deficiencies are provided by Fig. 11, which focuses on a specific El Niño event (2002–2003). From May to September 2002, the observed winter flow increased rapidly from 0.15 to 0.5 mm day^{-1} (Fig. 11a) in response to intense rainfall events (Fig. 11b) and gradual snowmelt (Fig. 11c). Most of this precipitation, however, served to refill the soil-moisture accounting (SMA) store of the model, which, after three years of intense La Niña-related drought (1999–2002), was only 15% of capacity (Fig. 11d). As a result, effective precipitation did not exceed 0.5 mm day^{-1} during this five-month period (Fig. 11e), of which only 10%, i.e. less than 0.05 mm day^{-1} , were processed through the quick flow routing path (Fig. 11f). The remaining 0.45 mm day^{-1} were added to the routing store, whose water level was also very low in May 2002. The overall quantity

11516

routed by both pathways was therefore largely insufficient to match the actual streamflow. A similar sequence was observed for all water years characterized by the same failures in streamflow predictions, shedding light on two critical sources of uncertainty.

5.3.1 Structural deficiencies

5 Arguably the largest source of structural uncertainty in the hydrological model lies in the representation of runoff production by a single SMA store. This lumps together quite distinct landscape units and misses a number of important differences in the functioning of upland and lowland areas. Of these differences the most notable relate to the terrain over which precipitation occurs. In the mountains, most of the land cover
10 is dominated by barren to sparsely vegetated exposed rocks, boulders and rubble. The topography is steep, with slopes as large as 30° and very poor soil development above the mountain front zone. By contrast, the valley bottoms appear as relatively flat areas largely covered by vegetation. Alluvial fans are also found along the mountain foothills, acting as hydrologic buffers between these two landscape units.

15 Another key difference arises from the type of precipitation involved. That it occurs mainly as snow in the uplands and rain in the lowlands is expected to have some consequences on the hydrological response of each landscape unit. Snowmelt typically occurs at a much lower and more consistent rate than rainfall, which means that much of the meltwater can be expected to soak into the ground. By contrast, high-
20 intensity rainstorms will tend to exceed the infiltration capacity and increase overland flow. This is especially the case in dryland areas where vegetation cover is sparse and rainfall events highly erratic. Additionally, rainfall events generally occur much closer to the catchment outlet than snowmelt and often not very far from the saturated riparian zone. This limits transmission losses and further enhances overland flow. Rain,
25 while not a dominant feature of semi-arid Andean catchments, can exert a significant influence on winter flows even during dry years. In the GR4J model, as in many other precipitation-runoff models, rainfall and snowmelt inputs are treated as the same kind of “water” and processed through the same pathways within the model structure. In

11517

reality, different types of precipitation will most likely involve different modes of runoff generation. By and large, a greater proportion of rainwater should be expected to bypass the SMA store in comparison to meltwater. This difference remains largely ignored by traditional lumped precipitation-runoff models.

5 Recent studies have suggested possible ways to make up for these structural deficiencies while preserving the overall simplicity of the lumped conceptual approach (e.g. Savenije et al., 2010; Gharari et al., 2014). In short, different SMA stores could be used in parallel to represent runoff production from different functional units (i.e. riparian zone, valley bottoms, mountain front, headwaters). The same routing module would
10 then be used to route the overall output from these various production modules. Investigating such modifications was far beyond the scope of this study and would greatly benefit from a comparison between multiple catchments.

5.3.2 Impacts of input data errors

15 Relatively high values were obtained for X1 (> 1000 mm) and X2 (~ 4 – 5 mm), which was somewhat surprising given our understanding of storage capacities and water fluxes in the Claro River catchment. The X2 parameter, in particular, is used to represent groundwater exchanges with the underlying aquifer and/or neighboring catchments. Positive values indicate a net water gain at the catchment scale whereas negative values relate to a net water loss. Le Moine et al. (2007) have shown from the
20 analysis of 1040 French catchments that alluvial aquifers are more likely to be associated with negative values of X2 whereas crystalline bedrocks tend to correlate with values centered on zero ($-5 \leq X2 \leq 5$). Over the long term, however, the value of X2 is expected to be zero if the catchment is a closed system.

25 In this catchment, the valley-fill aquifers that compose most of the groundwater flow system are bounded by large mountain blocks of granitic origin, which drastically limits inter-catchment flow paths. Ground water in the bedrock is typically found in fractures or joints, with a low storage capacity, and soils are, on the whole, poorly developed. As a result, low values of X1 and negative values of X2 would have seemed more

11518

“realistic”. Note that the autocorrelation structure of model residuals shown in Fig. 7 was also indicative of substantial storage errors in the hydrological model. This lack of physical realism suggests that other factors may be at play. Both of these parameters, indeed, are known to interact strongly with precipitation and evapotranspiration input errors (e.g. Andréassian et al., 2004; Oudin et al., 2006; Thyer et al., 2009). The capacity of the SMA store tends to increase in the presence of random precipitation errors or if precipitation is systematically over-estimated (Oudin et al., 2006). Likewise, an excessively high value of X_2 might indicate that potential evapotranspiration is over-estimated and/or precipitation under-estimated.

As in many mountainous catchments, some precipitation events occurring at high elevations may not be captured by the gauging network (< 3200 m a.s.l.) used to interpolate precipitation across the catchment. These occasional errors naturally add to systematic volume errors caused by wind, wetting and evaporation losses at the gauge level, leading to an overall underestimation of precipitation at the catchment scale. However, a large uncertainty also surrounds the estimation of elevation effects on precipitation. Mean annual precipitation was assumed to increase by $\sim 0.4 \text{ m we km}^{-1}$ (Sect. 2.2.1), yet in the absence of reliable precipitation data above 3200 m a.s.l., it is unclear whether this gradient under-estimated or over-estimated precipitation enhancement. In general, it is unlikely that a constant value would represent orographic effects correctly at all elevations and over the whole simulation period. Precipitation enhancement in the Andes can vary considerably on a year-to-year basis or from one event to another (Falvey and Garreaud, 2007), leading to time-varying errors in the estimation of precipitation inputs. From Fig. 6 we hypothesize that precipitation was on the whole underestimated, and only occasionally overestimated. Overestimation of potential evapotranspiration is also a plausible hypothesis for Models B and C owing to possible interactions with the estimation of sublimation rates and irrigation water-use (Fig. 7).

11519

5.4 Phenological modeling

Contrary to lumped catchment models, the phenological models used in this study allow for a direct interpretation of parameter values through comparison with existing experimental studies. This provides a second level of model validation.

The values obtained for T_{opt} (i.e. the optimal forcing temperature) with the full bloom and harvest models (Table 3) were generally close to the range of optimal photosynthetic temperatures reported in the literature, i.e. typically 20–30 °C (García de Cortázar-Atauri et al., 2010). On the contrary, relatively high values (around 11–12 °C) were found for parameter b (i.e. the optimal chilling temperature) compared to those reported by previous modeling and experimental (e.g. Fila et al., 2012) studies. Moreover, the values obtained for parameter a , which determines the range of acceptable chilling temperatures around the optimum b , imply that temperatures around 13–16 °C were still effective as chilling temperatures. Caffarra and Eccel (2010) and Fila et al. (2014) also found large effective chilling intervals with similar budburst models but different grapevine varieties, which they explained in different ways. In our case, this outcome was most likely related to the use of mean daily temperatures as inputs to the budburst model. Very high diurnal variations (~ 20 °C) can be observed at the INIA experimental site, where a mean temperature of 11–12 °C actually reflects temperatures close to 0 °C during several hours of the day. The critical states of chilling (C_{BB}) obtained for both varieties indicate that between 11 and 27 days at 11–12 °C were required to break endodormancy. Assuming that winter temperatures remained close to zero during at least 5 h per day, these results are fully consistent with the fact that most grapevine varieties typically require between 50 and 400 h at temperatures below 7 °C to achieve budburst (Fila et al., 2012). However, given the limited number of years with available observations and the absence of direct evidence for the release of endodormancy, possible trade-offs between the chilling (a , b , C_{BB}) and forcing (F_{BB}) parameters during the optimization process cannot be dismissed a priori. Thus, while the phenological models can be considered reliable under the conditions observed over 1985–2005, their

11520

- Ajami, N. K., Hornberger, G. M., and Sunding, D. L.: Sustainable water resource management under hydrological uncertainty, *Water Resour. Res.*, 44, W11406, doi:10.1029/2007WR006736, 2008.
- Allen, R. G., Smith, M., Perrier, A., and Pereira, L. S.: Crop evapotranspiration – guidelines for computing crop water requirements, Irrigation Drainage Paper 56, Food and Agric. Organ., Rome, Italy, 1998.
- Andréassian, V., Perrin, C., and Michel, C.: Impact of imperfect potential evapotranspiration knowledge on the efficiency and parameters of watershed models, *J. Hydrol.*, 286, 19–35, 2004.
- Ashagrie, A. G., de Laat, P. J., de Wit, M. J., Tu, M., and Uhlenbrook, S.: Detecting the influence of land use changes on discharges and floods in the Meuse River Basin – the predictive power of a ninety-year rainfall-runoff relation?, *Hydrol. Earth Syst. Sci.*, 10, 691–701, doi:10.5194/hess-10-691-2006, 2006.
- Ayala, A., McPhee, J., and Vargas, X.: Altitudinal gradients, midwinter melt, and wind effects on snow accumulation in semiarid midlatitude Andes under La Niña conditions, *Water Resour. Res.*, 50, 3589–3594, 2014.
- Ayala, A., Pellicciotti, F., MacDonell, S., McPhee, J., and Burlando, P.: Meteorological conditions associated to high sublimation amounts in semiarid high-elevation Andes decrease the performance of empirical melt models, EGU General Assembly 2015, 12–17 April 2015, Vienna, Austria, 2015.
- Beven, K., Smith, P. J., and Wood, A.: On the colour and spin of epistemic error (and what we might do about it), *Hydrol. Earth Syst. Sci.*, 15, 3123–3133, doi:10.5194/hess-15-3123-2011, 2011.
- Blöschl, G. and Montanari, A.: Climate change impacts – throwing the dice?, *Hydrol. Process.*, 24, 374–381, 2010.
- Boudhar, A., Hanich, L., Boulet, G., Duchemin, B., Berjamy, B., and Chehbouni, A.: Evaluation of the Snowmelt Runoff Model in the Moroccan High Atlas Mountains using two snow-cover estimates, *Hydrolog. Sci. J.*, 54, 1094–1113, 2009.
- Bourgin, P.-Y., Andréassian, V., Gascoin, S., and Valéry, A.: Que sait-on des précipitations en altitude dans les Andes semi-arides du Chili?, *Houille Blanche*, 2, 12–17, 2012.
- Brigode, P., Oudin, L., and Perrin, C.: Hydrological model parameter instability: a source of additional uncertainty in estimating the hydrological impacts of climate change?, *J. Hydrol.*, 476, 410–425, 2013.

11523

- Brubaker, K., Rango, A., and Kustas, W.: Incorporating radiation inputs into the snowmelt runoff model, *Hydrol. Process.*, 10, 1329–1343, 1996.
- Caffarra, A. and Eccel, E.: Increasing the robustness of phenological models for *Vitis vinifera* cv. Chardonnay, *Int. J. Biometeorol.*, 54, 255–267, 2010.
- Caffarra, A. and Eccel, E.: Projecting the impacts of climate change on the phenology of grapevine in a mountain area, *Aust. J. Grape Wine R.*, 17, 52–61, 2011.
- Chuine, I.: A unified model for budburst of trees, *J. Theor. Biol.*, 207, 337–347, 2000.
- Cleland, E. E., Chuine, I., Menzel, A., Harold, A. M., and Schwartz, M. D.: Shifting plant phenology in response to global change, *Trends Ecol. Evol.*, 22, 357–365, 2007.
- Collet, L., Ruelland, D., Borrell-Estupina, V., Dezetter, A., and Servat, E.: Water supply sustainability and adaptation strategies under future anthropogenic and climatic changes of a meso-scale catchment, *Sci. Total Environ.*, 536, 589–602, 2015.
- Craufurd, P. Q. and Wheeler, T. R.: Climate change and the flowering time of annual crops, *J. Exp. Bot.*, 60, 2529–2539, 2009.
- Duan, Q. Y., Gupta, V. K., and Sorooshian, S.: A shuffled complex evolution approach for effective and efficient global minimization, *J. Optimiz. Theory App.*, 76, 501–521, 1993.
- Duchêne, E. and Schneider, C.: Grapevine and climatic changes: a glance at the situation in Alsace, *Agron. Sustain. Dev.*, 25, 93–99, 2010a.
- Duchêne, E., Huard, F., Dumas, V., Schneider, C., and Merdinoglu, D.: The challenge of adapting grapevine varieties to climate change, *Clim. Res.*, 41, 193–204, 2010b.
- Engeland, K., Renard, B., Steinsland, I., and Kolberg, S.: Evaluation of statistical models for forecast errors from the HBV model, *J. Hydrol.*, 384, 142–155, 2010.
- Fabre, J., Ruelland, D., Dezetter, A., and Grouillet, B.: Accounting for hydro-climatic and water-use variability in the assessment of past and future water balance at the basin scale, in: Hydrologic Non-stationarity and Extrapolating Models to Predict the Future, Proc. of symp. HS02 held during IUGG2015 in Prague, Czech Republic, June 2015b, IAHS Publ., 371, 43–48, 2015a.
- Fabre, J., Ruelland, D., Dezetter, A., and Grouillet, B.: Simulating past changes in the balance between water demand and availability and assessing their main drivers at the river basin scale, *Hydrol. Earth Syst. Sci.*, 19, 1263–1285, doi:10.5194/hess-19-1263-2015, 2015b.
- Falvey, M. and Garreaud, R. D.: Wintertime precipitation episodes in central Chile: associated meteorological conditions and orographic influences, *J. Hydrometeorol.*, 8, 171–193, 2007.

11524

- Favier, V., Falvey, M., Rabatel, A., Praderio, E., and López, D.: Interpreting discrepancies between discharge and precipitation in high-altitude area of Chile's Norte Chico region (26–32° S), *Water Resour. Res.*, 45, W02424, doi:10.1029/2008WR006802, 2009.
- Fenicia, F., Kavetski, D., and Savenije, H. H. G.: Elements of a flexible approach for conceptual hydrological modeling: 1. Motivation and theoretical development, *Water Resour. Res.*, 47, W11510, doi:10.1029/2010WR010174, 2011.
- Fila, G., Di Lena, B., Gardiman, M., Storch, P., Tomasi, D., Silvestroni, O., and Pitacco, A.: Calibration and validation of grapevine budburst models using growth-room experiments as data source, *Agr. Forest Meteorol.*, 160, 69–79, 2012.
- Fila, G., Gardiman, M., Belvini, P., Meggio, F., and Pitacco, A.: A comparison of different modelling solutions for studying grapevine phenology under present and future climate scenarios, *Agr. Forest Meteorol.*, 195–196, 192–205, 2014.
- Fontaine, T. A., Cruickshank, T. S., Arnold, J. G., and Hotchkiss, R. H.: Development of a snowfall-snowmelt routine for mountainous terrain for the soil water assessment tool (SWAT), *J. Hydrol.*, 262, 209–223, 2002.
- García de Cortázar-Atauri, I., Daux, V., Garnier, E., Yiou, P., Viovy, N., Seguin, B., Bourisquot, J. M., Parker, A. K., van Leeuwen, C., and Chuine, I.: Climate reconstructions from grape harvest dates: methodology and uncertainties, *Holocene*, 20, 599–608, 2010.
- Gascoïn, S., Lhermitte, S., Kinnard, C., Bortels, K., and Liston, G. E.: Wind effects on snow cover in Pascua-Lama, dry Andes of Chile, *Adv. Water Resour.*, 55, 25–39, 2013.
- Gelman, A. G. and Rubin, D. B.: Inference from iterative simulation using multiple sequences, *Stat. Sci.*, 7, 457–472, 1992.
- Gharari, S., Hrachowitz, M., Fenicia, F., Gao, H., and Savenije, H. H. G.: Using expert knowledge to increase realism in environmental system models can dramatically reduce the need for calibration, *Hydrol. Earth Syst. Sci.*, 18, 4839–4859, doi:10.5194/hess-18-4839-2014, 2014.
- Greer, D. H. and Weedon, M. M.: The impact of high temperatures on *Vitis vinifera* cv, Semillon grapevine performance and berry ripening, *Front. Plant Sci.*, 4, 491, 2013.
- Gupta, H. V., Kling, H., Yilmaz, K. K., and Martinez, G. F.: Decomposition of the mean squared error and NSE performance criteria: implications for improving hydrological modelling, *J. Hydrol.*, 377, 80–91, 2009.

11525

- Harshburger, B. J., Humes, K. S., Walden, V. P., Moore, B. C., Blandford, T. R., and Rango, A.: Evaluation of short-to-medium range streamflow forecasts obtained using an enhanced version of SRM, *J. Am. Water Resour. As.*, 46, 603–617, 2010.
- Hendrickson, L., Ball, M. C., Wood, J. T., Chow, W. S., and Furbank, R. T.: Low temperature effects on photosynthesis and growth of grapevine, *Plant Cell Environ.*, 27, 795–809, 2004.
- Hock, R.: Temperature index melt modelling in mountain areas, *J. Hydrol.*, 282, 104–115, 2003.
- Hublart, P., Ruelland, D., Dezetter, A., and Jourde, H.: Reducing structural uncertainty in conceptual hydrological modelling in the semi-arid Andes, *Hydrol. Earth Syst. Sci.*, 19, 2295–2314, doi:10.5194/hess-19-2295-2015, 2015.
- Hughes, D. A. and Mantel, S. K.: Estimating the uncertainty in simulating the impacts of small farm dams on streamflow regimes in South Africa, *Hydrolog. Sci. J.*, 55, 578–592, 2010.
- Ibacache, A.: Cómo influye la temperatura sobre la época de cosecha en vides, *Tierra Adentro*, 81, 8–10, 2008.
- Ibacache, A., Martínez, L., Sturla, C., and Montes, C.: Zonificación del territorio de la denominación de origen Pisco, *Nuestro Pisco*, Programa de Innovación Territorial, Informe Final, Publ. Nuestro Pisco, IV Región de Coquimbo, Chile, 2010.
- Jin, X., Xu, C.-Y., Zhang, Q., and Singh, V. P.: Parameter and modeling uncertainty simulated by GLUE and a formal Bayesian method for a conceptual hydrological model, *J. Hydrol.*, 383, 147–155, 2010.
- Jones, G. V., White, M. A., Cooper, O. R., and Storchmann, K.: Climate change and global wine quality, *Climatic Change*, 73, 319–343, 2005.
- Kalthoff, N., Fiebig-Wittmaack, M., Meißner, C., Kohler, M., Uriarte, M., Bischoff-Gauß, I., and Gonzales, E.: The energy balance, evapo-transpiration and nocturnal dew deposition of an arid valley in the Andes, *J. Arid Environ.*, 65, 420–443, 2006.
- Kim, H. S., Croke, B. F. W., Jakeman, A. J., Chiew, F., and Mueller, N.: Towards separation of climate and land use effects on hydrology: data analysis of the Googong and Cotter Catchments, in: MODSIM 2007 International Congress on Modelling and Simulation, Modelling and Simulation Society of Australia and New Zealand, edited by: Oxley, L., and Kulasiri, D., 74–80, 2007.
- Kiptala, J. K., Mul, M. L., Mohamed, Y. A., and van der Zaag, P.: Modelling stream flow and quantifying blue water using a modified STREAM model for a heterogeneous, highly utilized and data-scarce river basin in Africa, *Hydrol. Earth Syst. Sci.*, 18, 2287–2303, doi:10.5194/hess-18-2287-2014, 2014.

11526

- Koskela, J. J., Croke, B. W. F., Koivusalo, H., Jakeman, A. J., and Kokkonen, T.: Bayesian inference of uncertainties in precipitation-streamflow modeling in a snow affected catchment, *Water Resour. Res.*, 48, W11513, doi:10.1029/2011WR011773, 2012.
- Laio, F. and Tamea, S.: Verification tools for probabilistic forecasts of continuous hydrological variables, *Hydrol. Earth Syst. Sci.*, 11, 1267–1277, doi:10.5194/hess-11-1267-2007, 2007.
- 5 Le Moine, N., Andréassian, V., Perrin, C., and Michel, C.: How can rainfall–runoff models handle intercatchment groundwater flows? Theoretical study based on 1040 French catchments, *Water Resour. Res.*, 43, W06428, doi:10.1029/2006WR005608, 2007.
- Lhermitte, S., Abermann, J., and Kinnard, C.: Albedo over rough snow and ice surfaces, *The Cryosphere*, 8, 1069–1086, doi:10.5194/tc-8-1069-2014, 2014.
- 10 L'hôte, Y., Chevallier, P., Coudrain, A., Lejeune, Y., and Etchevers, P.: Relationship between precipitation phase and air temperature: comparison between the Bolivian Andes and the Swiss Alps, *Hydrolog. Sci. J.*, 50, 989–997, 2005.
- MacDonell, S., Kinnard, C., Mölg, T., Nicholson, L., and Abermann, J.: Meteorological drivers of ablation processes on a cold glacier in the semiarid Andes of Chile, *The Cryosphere Discuss.*, 7, 1833–1870, doi:10.5194/tcd-7-1833-2013, 2013.
- 15 McIntyre, N., Ballard, C., Bruen, M., Bulygina, N., Buytaert, W., Cluckie, I., Dunn, S., Ehret, U., Ewen, J., Gelfan, A., Hess, T., Hughes, D., Jackson, B., Kjeldsen, T. R., Merz, R., Park, J.-S., O'Connell, E., O'Donnell, G., Oudin, L., Todini, E., Wagener, T., and Wheeler, H.: Modelling the hydrological impacts of rural land use change, *Hydrol. Res.*, 45, 737–754, 2014.
- 20 Merritt, W. S., Croke, B. F. W., Jakeman, A. J., Letcher, R. A., and Perez, P.: A biophysical toolbox for assessment and management of land and water resources in rural catchments in northern Thailand, *Ecol. Model.*, 171, 279–300, 2004.
- Montecinos, A. and Aceituno, P.: Seasonality of the ENSO-related rainfall variability in central Chile and associated circulation anomalies, *J. Climate*, 16, 281–296, 2003.
- 25 Nicolle, P., Pushpalatha, R., Perrin, C., François, D., Thiéry, D., Mathevet, T., Le Lay, M., Besson, F., Soubeyroux, J.-M., Viel, C., Regimbeau, F., Andréassian, V., Maugis, P., Augéard, B., and Morice, E.: Benchmarking hydrological models for low-flow simulation and forecasting on French catchments, *Hydrol. Earth Syst. Sci.*, 18, 2829–2857, doi:10.5194/hess-18-2829-2014, 2014.
- 30 Ohlanders, N., Rodriguez, M., and McPhee, J.: Stable water isotope variation in a Central Andean watershed dominated by glacier and snowmelt, *Hydrol. Earth Syst. Sci.*, 17, 1035–1050, doi:10.5194/hess-17-1035-2013, 2013.

11527

- Ohmura, A.: Physical basis for the temperature-based melt-index method, *J. Appl. Meteorol.*, 40, 753–761, 2001.
- Oudin, L., Hervieu, F., Michel, C., Perrin, C., Andréassian, V., Anctil, F., and Loumagne, C.: Which potential evapotranspiration input for a lumped rainfall–runoff model? Part 2: Towards a simple and efficient potential evapotranspiration model for rainfall–runoff modelling, *J. Hydrol.*, 303, 290–306, 2005.
- 5 Oudin, L., Perrin, C., Mathevet, T., Andréassian, V., and Michel, C.: Impact of biased and randomly corrupted inputs on the efficiency and the parameters of watershed models, *J. Hydrol.*, 320, 62–83, 2006.
- 10 Palliotti, A., Tombesi, S., Silvestroni, O., Lanari, V., Gatti, M., and Poni, S.: Changes in vineyard establishment and canopy management urged by earlier climate-related grape ripening: a review, *Sci. Hort.*, 178, 43–54, 2014.
- Parker, A., Garcia de Cortázar-Atauri, I., Chuine, I., Barbeau, G., Bois, B., Boursiquot, J. M., Cahurel, J. Y., Claverie, M., Dufourcq, T., Génys, L., Guimberteau, G., Hofmann, R. W., Jacquet, O., Lacombe, T., Monamy, C., Ojeda, H., Panigai, L., Payan, J. C., Lovelle, B. R., Rouchaud, E., Schneider, C., Spring, J. L., Storchi, P., Tomasi, D., Trambouze, W., Trought, M., and van Leeuwen, C.: Classification of varieties for their timing of flowering and veraison using a modelling approach: a case study for the grapevine species *Vitis vinifera* L., *Agr. Forest Meteorol.*, 180, 249–264, 2013.
- 15 Pellicciotti, F., Helbing, J., Rivera, A., Favier, V., Corripio, J., Araos, J., Sicart, J. E., and Carenzo, M.: A study of the energy balance and melt regime on Juncal Norte Glacier, semiarid Andes of central Chile, using melt models of different complexity, *Hydrol. Process.*, 22, 3980–3997, 2008.
- Perrin, C., Michel, C., and Andréassian, V.: Improvement of a parsimonious model for streamflow simulation, *J. Hydrol.*, 279, 275–289, 2003.
- 25 Pushpalatha, R., Perrin, C., Le Moine, N., and Andréassian, V.: A downward structural sensitivity analysis of hydrological models to improve low-flow simulation, *J. Hydrol.*, 411, 66–76, 2011.
- Pushpalatha, R., Perrin, C., Le Moine, N., Mathevet, T., and Andréassian, V.: A review of efficiency criteria suitable for evaluating low-flow simulations, *J. Hydrol.*, 420–421, 171–182, 2012.
- 30 Ruelland, D., Dezetter, A., and Hublart, P.: Sensitivity analysis of hydrological modelling to climate forcing in a semi-arid mountainous catchment, in: *Hydrology in a Changing World: Envi-*

11528

- ronmental and Human Dimensions, Proc. 7th FRIEND-Water Int. Conf., Montpellier, France, 7–10 October 2014, IAHS Publ., 363, 145–150, 2014.
- Salinas, C. X., Gironás, J., and Pinto, M.: Water security as a challenge for the sustainability of La Serena-Coquimbo conurbation in northern Chile: global perspectives and adaptation, *Mitig. Adapt. Strateg. Glob. Change*, doi:10.1007/s11027-015-9650-3, in press, 2015.
- 5 Savenije, H. H. G.: HESS Opinions “Topography driven conceptual modelling (FLEX-Topo)”, *Hydrol. Earth Syst. Sci.*, 14, 2681–2692, doi:10.5194/hess-14-2681-2010, 2010.
- Scanlon, B. R., Keese, K. E., Flint, A. L., Flint, L. E., Gaye, C. B., Edmunds, M. W., and Simmers, I.: Global synthesis of groundwater recharge in semiarid and arid regions, *Hydrol. Process.*, 20, 3335–3370, 2006.
- 10 Schaeffli, B. and Huss, M.: Integrating point glacier mass balance observations into hydrologic model identification, *Hydrol. Earth Syst. Sci.*, 15, 1227–1241, doi:10.5194/hess-15-1227-2011, 2011.
- Schoups, G. and Vrugt, J. A.: A formal likelihood function for parameter and predictive inference of hydrologic models with correlated, heteroscedastic, and non-Gaussian errors, *Water Resour. Res.*, 46, W10531, doi:10.1029/2009WR008933, 2010.
- 15 Schulz, N., Boisier, J. P., and Aceituno, P.: Climate change along the arid coast of northern Chile, *Int. J. Climatol.*, 32, 1803–1814, 2011.
- Schulz, O. and de Jong, C.: Snowmelt and sublimation: field experiments and modelling in the High Atlas Mountains of Morocco, *Hydrol. Earth Syst. Sci.*, 8, 1076–1089, doi:10.5194/hess-8-1076-2004, 2004.
- 20 Seibert, J. and McDonnell, J. J.: Land-cover impacts on streamflow: a change-detection modelling approach that incorporates parameter uncertainty, *Hydrolog. Sci. J.*, 55, 316–332, 2010.
- Siebert, S. and Döll, P.: Quantifying blue and green virtual water contents in global crop production as well as potential production losses without irrigation, *J. Hydrol.*, 384, 198–217, 2010.
- 25 Smith, T., Sharma, A., Marshall, L., Mehrotra, R., and Sisson, S.: Development of a formal likelihood function for improved Bayesian inference of ephemeral catchments, *Water Resour. Res.*, 46, W12551, doi:10.1029/2010WR009514, 2010.
- 30 Sproles, E. A., Nolin, A. W., Rittger, K., and Painter, T. H.: Climate change impacts on maritime mountain snowpack in the Oregon Cascades, *Hydrol. Earth Syst. Sci.*, 17, 2581–2597, doi:10.5194/hess-17-2581-2013, 2013.

11529

- Squeo, F. A., Veit, H., Arancio, G., Gutiérrez, J. R., Arroyo, M. T. K., and Olivares, N.: Spatial heterogeneity of high mountain vegetation in the Andean desert zone of Chile (30° S), *Mt. Res. Dev.*, 13, 203–209, 1993.
- Staudinger, M., Stahl, K., Seibert, J., Clark, M. P., and Tallaksen, L. M.: Comparison of hydrological model structures based on recession and low flow simulations, *Hydrol. Earth Syst. Sci.*, 15, 3447–3459, doi:10.5194/hess-15-3447-2011, 2011.
- 5 Stehr, A., Debels, P., Arumi, J. L., Romero, F., and Alcayaga, H.: Combining the Soil and Water Assessment Tool (SWAT) and MODIS imagery to estimate monthly flows in a datascarc Chilean Andean basin, *Hydrolog. Sci. J.*, 54, 1053–1067, 2009.
- 10 Thyer, M., Renard, B., Kavetski, D., Kuczera, G., Franks, S. W., and Srikanthan, S.: Critical evaluation of parameter consistency and predictive uncertainty in hydrological modeling: a case study using Bayesian total error analysis, *Water Resour. Res.*, 45, W00B14, doi:10.1029/2008WR006825, 2009.
- 15 Valéry, A.: Modélisation précipitations – débit sous influence nivale Elaboration d’un module neige et évaluation sur 380 bassins versants, PhD Thesis, AgroParisTech, Irstea, Paris, 2010.
- Valéry, A., Andréassian, V., and Perrin, C.: Regionalization of precipitation and air temperature over high-altitude catchments – learning from outliers, *Hydrolog. Sci. J.*, 55, 928–940, 2010.
- 20 Valéry, A., Andréassian, V., and Perrin, C.: As simple as possible but not simpler: what is useful in a temperature-based snow-accounting routine? Part 2 – Sensitivity analysis of the Cemanegige snow accounting routine on 380 catchments, *J. Hydrol.*, 517, 1176–1187, 2014.
- Verbist, K., Robertson, A. W., Cornelis, W. M., and Gabriels, D.: Seasonal predictability of daily rainfall characteristics in central northern Chile for dry-land management, *J. Appl. Meteorol. Clim.*, 49, 1938–1955, 2010.
- 25 Villagra, P., García de Cortázar, V., Ferreyra, R., Aspillaga, C., Zúñiga, C., Ortega-Farías, S., and Sellés, G.: Estimation of water requirements and Kc values of “Thompson Seedless” table grapes grown in the overhead trellis system, using the Eddy covariance method, *Chil. J. Agr. Res.*, 74, 213–218, 2014.
- 30 Vrugt, J. A., ter Braak, C. J. F., Diks, C. G. H., Higdon, D., Robinson, B. A., and Hyman, J. M.: Accelerating Markov chain Monte Carlo simulation by differential evolution with self-adaptive randomized subspace sampling, *Int. J. Nonlin. Sci. Num.*, 10, 271–288, 2009.

11530

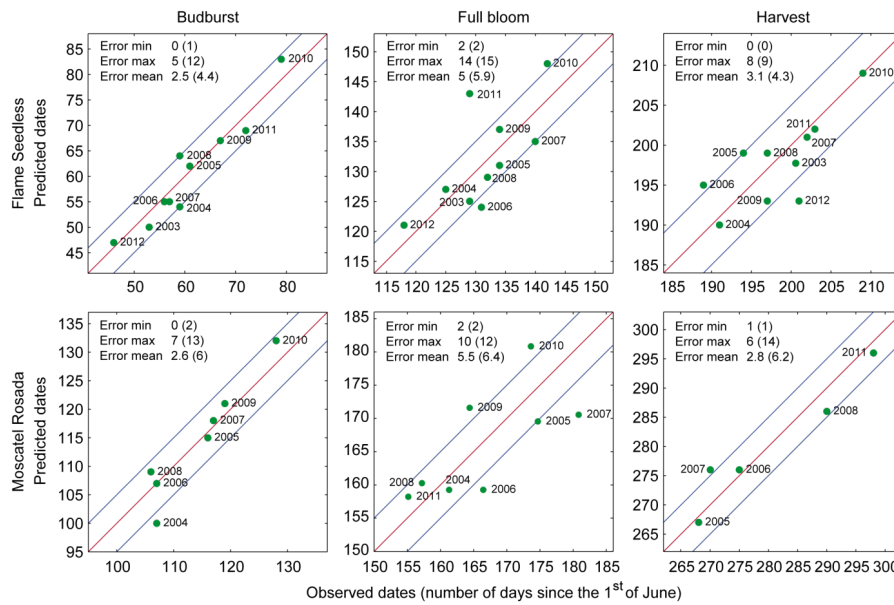


Figure 5. Observed vs. predicted dates of budburst, full bloom and harvest for flame seedless and moscatel rosada at the INIA experimental site. The dates are expressed in number of days since the 1 June. The minimum, maximum and mean absolute errors (in days) are given for each variety and stage of growth (the values between brackets relate to the validation step while the values in front of the brackets relate to the calibration step). The upper and lower blue lines indicate delays of ± 5 days between observed and predicted dates, respectively.

11541

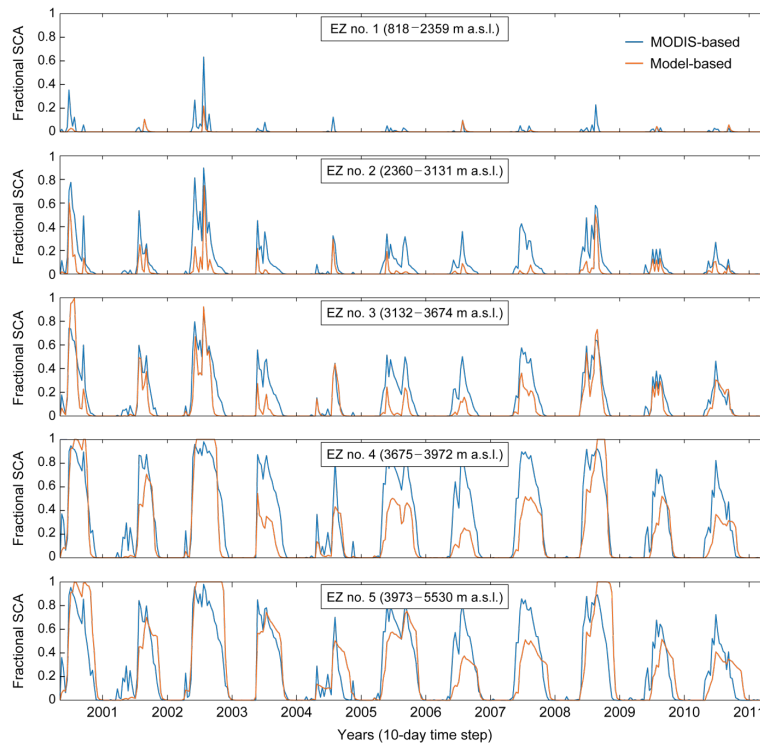


Figure 6. Comparison of simulated (i.e. Model C, accounting for sublimation) and observed (i.e. MODIS-based) fractional snow-covered areas (validation period). The graduations on the x axis indicate the 1 January of each year.

11542

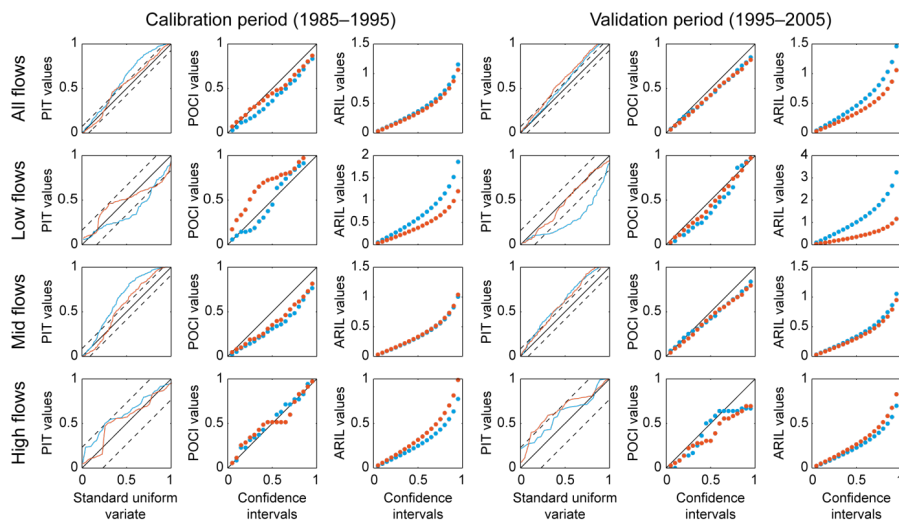


Figure 9. Posterior diagnostics used to evaluate the reliability (PIT, POCI) and resolution (ARIL) of the forecast distributions obtained with Model B (in blue) and Model C (in red).

11545

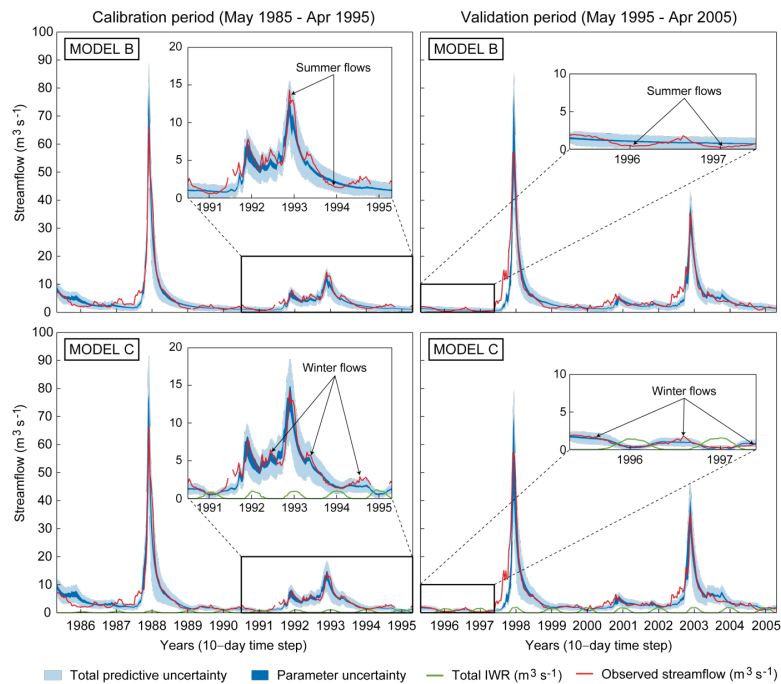


Figure 10. Predictive uncertainty bands obtained for both models with the DREAM algorithm and GL function. The dark blue region represents the 95 % confidence intervals associated with parameter uncertainty, whereas the light blue region represents the 95 % confidence intervals associated with parameter, model structure and input errors. The graduations on the x axis indicate the 1 January of each year.

11546

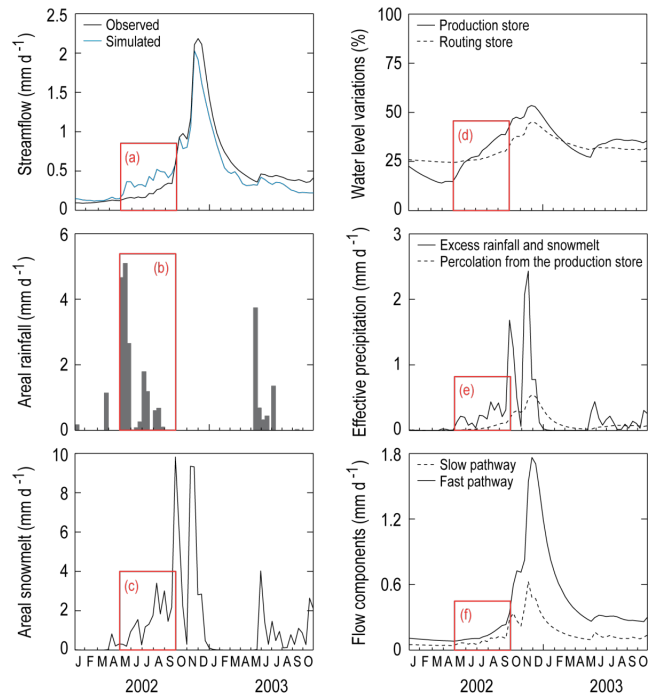


Figure 11. Internal state variables and fluxes obtained with Model C during the 2002–03 El Niño event (using the best-performing parameter set obtained by calibration against the F_{obj} function).

11547

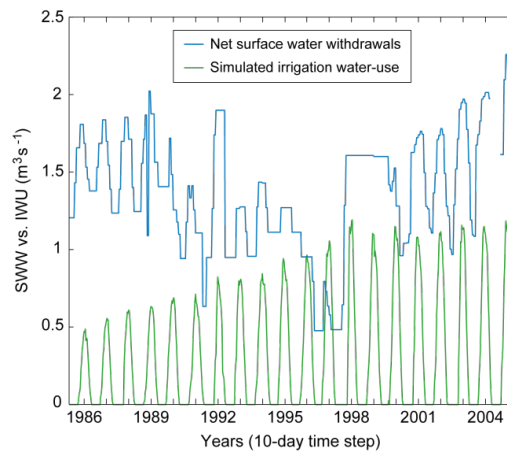


Figure 12. Comparison of net surface-water withdrawals (SWW) and irrigation water-use (IWU) at the catchment scale: SWW were obtained by considering monthly restrictions to water access entitlements provided by the Chilean authorities, a conveyance efficiency of 0.6 and a field application efficiency of 0.6 for pisco varieties and 0.9 for table varieties; IWU was obtained from model simulations.

11548